The dynamics of a seismic wave field: Animation and analysis of kinematic GPS data recorded during the 2011 Tohoku-oki earthquake, Japan

Ronni Grapenthin[1] and Jeffrey T. Freymueller[1]

Received 20 June 2011; revised 23 August 2011; accepted 25 August 2011; published 22 September 2011.

[1] During rupture, earthquakes induce permanent and dynamic ground displacements that can be measured by GPS. More than 1200 continuous GPS stations distributed throughout Japan recorded the displacements due to the March 11, 2011, M_w9.0 Tohoku-oki earthquake. We animate these data, which shows the growth of the earthquake rupture over time and illustrates differences of earthquake magnitude through two smaller aftershocks. We also identify dynamic ground motion due to S-waves (body waves), Love waves and Rayleigh waves (surface waves) in this data set. Real time availability of such displacements could be of great use in earthquake response and tsunami warning, and to some degree in earthquake early warning. We find that the length of the ruptured fault can be approximated from displacements which could allow rapid identification of areas prone to large aftershocks. We outline a method that integrates real time displacements into an earthquake alarm system. The animated displacements in map view are easily understandable by specialists and non-specialists alike and hence provide a valuable education and outreach tool.
Citation: Grapenthin, R., and J. T. Freymueller (2011), The dynamics of a seismic wave field: Animation and analysis of kinematic GPS data recorded during the 2011 Tohoku-oki earthquake, Japan, *Geophys. Res. Lett.*, *38*, L18308, doi:10.1029/2011GL048405.

1. Introduction

[2] Earthquakes displace the ground during rupture and create seismic waves, which induce dynamic displacements that travel around the globe. Within the last decade, high-rate kinematic Global Positioning System (GPS) methods [*Larson et al.*, 2003] have been developed to provide ground displacements complementary to seismic records. However, due to sparse station coverage, such data are traditionally presented as time series for a few GPS stations, which neglects spatial correlation in the signal presentation. The uniquely dense Japanese GPS Earth Observation System (GEONET)[*Sagiya*, 2004] provided an impressive amount of data for the 05:46:23 UTC, March 11, 2011, M_w9.0 Tohoku-oki earthquake (source: USGS, http://earthquake.usgs.gov/earthquakes). Here, we visualize and analyze the vector field of directly measured dynamic and permanent displacements induced by this event and recorded by GEONET. The result is a map view movie of an earthquake (Figure 1 and Animations S1–S3 in the auxiliary material), which proves to be a valuable education and outreach tool as confirmed by early users and from our own experience.[1]

[3] Basic tools such as direct visualization of displacements in near real time can be crucial to estimate characteristics of big earthquakes such as magnitude and rupture length, which helps to identify regions that might be subject to large aftershocks. Furthermore, automated analysis of real time displacements could be useful in: (1) earthquake response to create products such as damage potential maps; (2) earthquake early warning [*Fleming et al.*, 2009; *Crowell et al.*, 2009], when geocorrelated permanent displacements near the epicenter are used for event detection; and (3) tsunami warning as the onshore static deformation field indicates changes in topography and bathymetry as soon as the body waves have passed (Figures 1b and 1c and Animation S3) and hence informs about the tsunami generation mechanism.

2. Data and Processing

[4] The GEONET raw data is currently not generally accessible from outside Japan, but the immediate implementation of the Tohoku-oki event website (GEO Supersites, http://supersites.earthobservations.org/sendai.php) allowed us to access three-dimensional 30 s kinematic position estimates produced by the ARIA project [*Simons et al.*, 2011] for all available GEONET sites. This open process enhanced opportunities for scientific collaboration and allowed for timely outreach to the general public.

[5] The ARIA team used the GIPSY software developed at NASA's Jet Propulsion Laboratory (JPL) to compute the kinematic displacements based on RINEX data provided to Caltech by the Geospatial Information Authority (GSI) of Japan. They provided a time series of displacements relative to the first epoch solution (2011/03/11, 00:00:00 UTC). We visualized displacements from 05:40:00–06:25:00 UTC using the complete dataset except stations 0197, 0228, 0550, and 0616, which appear noisy throughout the day. We reduced site specific jitter resulting from poorly determined epochs by setting the displacements at a station to zero if the provided uncertainty of an epoch position exceeds 0.25 m. The displacements were then reformatted for compatibility with the Generic Mapping Tools (GMT) [*Wessel and Smith*, 1995], which we used to create the individual frames of the animations. The resulting Postscript files were rasterized using ImageMagick's convert program. We cloned each frame 7 times to support the minimum frame rate of 12 frames per second required by some video players as well as to accommodate our wish for a slow animation. We concatenated the

[1]Geophysical Institute, University of Alaska Fairbanks, Fairbanks, Alaska, USA.

0094-8276/11/2011GL048405

[1]Auxiliary materials are available in the HTML. doi:10.1029/2011GL048405.

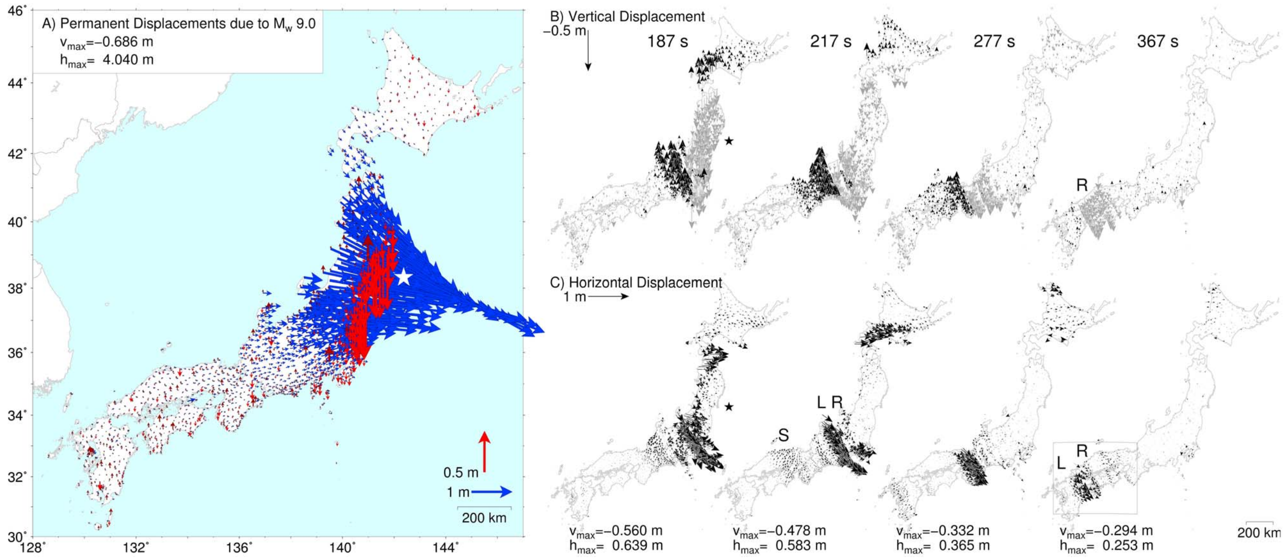

Figure 1. Permanent and dynamic displacements due to the M_w9.0 Tohoku-oki Earthquake. (a) Permanent displacements after the M_w9.0 earthquake (star marks epicenter). Maximum horizontal (blue arrows) and vertical (red arrows) displacements are given in inset. Vertical displacements are almost all subsidence, which means that all slip-induced uplift occurred off-shore. These permanent displacements are subtracted from Figures 1b and 1c to highlight the propagating seismic waves. (b, c) Vertical displacements (black: uplift, gray: subsidence) and horizontal displacements from 187–367 s after rupture initiation. Note that the full rupture took about 180 s (Figure 3). 'S', 'L', and 'R' indicate S-wave, Love wave, and Rayleigh wave, respectively. For each time maximum horizontal and vertical displacements are given below the respective panel. Box in Figure 1c indicates the location for Figures 2a–2d.

frames into animations with the software mencoder using the video codec msmpeg4v2 at a bit rate of 5320 kb. The animations were converted from avi to mp4 (Quicktime) format with the ffmpeg software. All software used is freely available and licensed under the GNU General Public License version 2. Generating a single rasterized frame takes about 2 seconds on a laptop with a 2.2 GHz Duo Core CPU processor and 2 GB memory. Half of this time is required for rasterization of the Postscript file. This is acceptable for the used 30 s solutions, but some optimization is necessary when 1 Hz real time data are used.

[6] In addition to animating the filtered data (Animation S1), which could be done in near real time, we provide two animations in which we remove the permanent displacements due to the mainshock (Figure 1a) at 05:55:30 UTC (Animation S2) and 05:49:30 UTC (Animation S3), respectively. These highlight aftershocks and seismic wave propagation, respectively, but potentially introduce distortions in the near field while permanent displacements are still accumulating. We advise comparison to Animation S1 before drawing conclusions about near-field features from Animations S2 and S3.

3. Results

[7] Some key features of the animations are illustrated in Figure 1. The permanent displacements (Figure 1a) caused by the M_w9.0 main shock are subtracted in Figures 1b and 1c to show vertical (Figure 1b) and horizontal (Figure 1c) dynamic displacement fields from 187 s–367 s after rupture initiation. We can clearly identify S-waves (body waves), Love waves and Rayleigh waves (surface waves) (Figures 2 and 3). The S-waves are best resolved in the horizontal field (Figure 2a). They radiate outwards from the source at an apparent velocity of 6–8 km/s in a swath of about 250 km width. This apparent velocity is not the actual S-wave propagation velocity (≈4.5 km/s in upper mantle), as the waves arriving at each point on the surface took different paths. However, from these values we can infer that each individual point is affected by large amplitude S-waves for at least 31–42 s while the wavetrain traverses Japan in 4.5–5 minutes. The S-wave duration of 31–42 s may be underestimated as the high moment-rate lasted about 50 s [*Ide et al.*, 2011], which should be proportional to body-wave excitation. Some stations may be in a phase similar to their reference position, so a single snapshot at a 30 s sample rate may not accurately show the full extent of the region where S-wave amplitudes are large. The Love wave that follows is also clearly resolved in the horizontal field. It displays a distinctive wave-front defined by its 'snake like' motion transverse to the direction of wave propagation. This wave-front travels about 270 km in 60 s at an estimated velocity of 4–5 km/s (Figure 2b). As Love waves cause horizontal displacements only, GPS data naturally separate them from the slower Rayleigh waves (Figures 2b–2d), which induce ellipsoidal particle motion up and parallel to the propagation direction. We estimate the Rayleigh wave to be about 0.35–0.42 km/s slower than the Love wave, which traveled 130 km farther in 367 s (Figure 2d). The surface waves take about 8.5–9 minutes to fully traverse Japan.

[8] The animations also capture the main rupture in 6 frames (Figure 3), which show the displaced region growing to the south as the rupture propagates. Surface displacement on land begins between 37 s and 67 s after rupture initiation (Origin time USGS, http://earthquake.usgs.gov/earthquakes). Large displacements are not observed until the epoch 97 s after

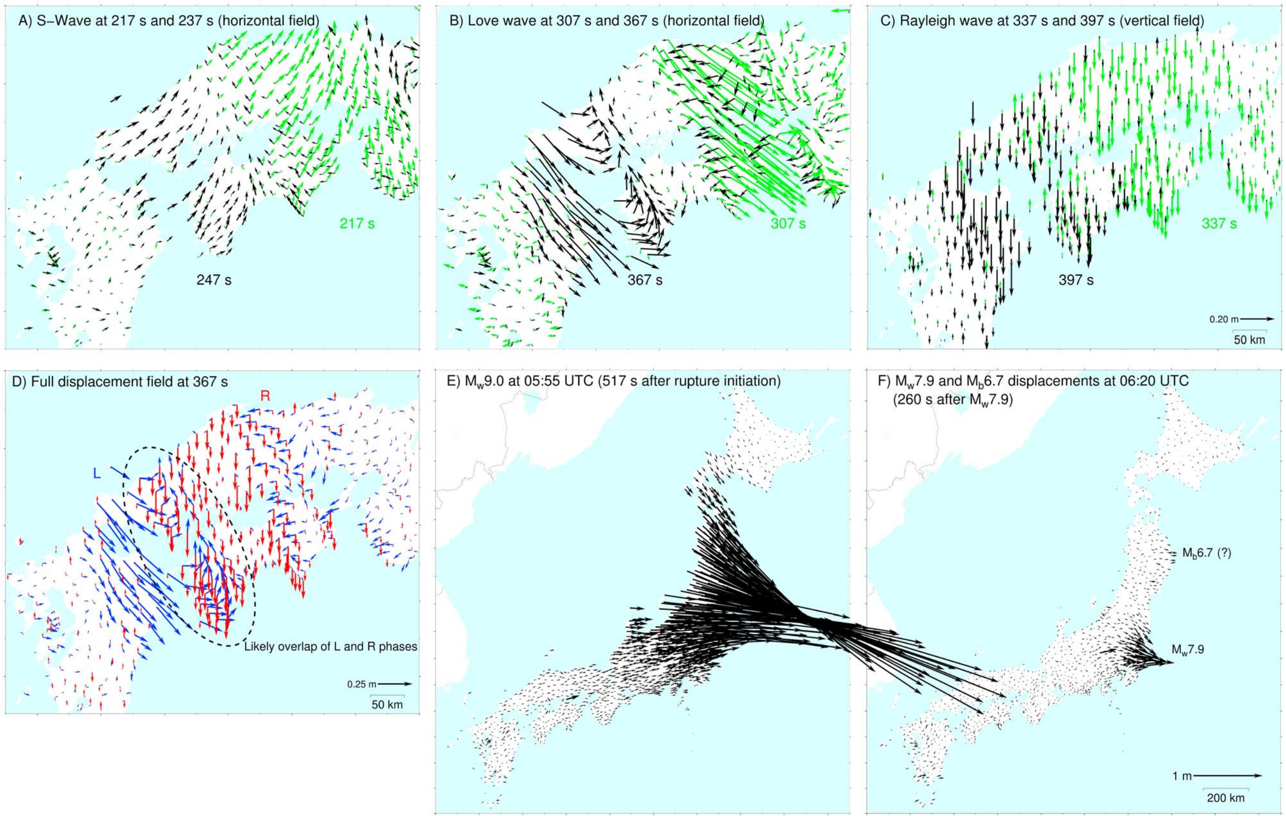

Figure 2. (a–c) Three wave patterns observed in the kinematic GPS data. The 3 observed wave patterns as they propagate through the box in Figure 1c; times are relative to origin time. Early records are green, later ones are black. (a) S-wave. (b) Love wave; note the well-defined displacements perpendicular to the propagation direction. The trailing smaller black arrows indicate the following Rayleigh wave (see Figure 2d). (c) Rayleigh wave. (d) The Love wave ('L') and Rayleigh Wave ('R'). Horizontal displacements (blue) and vertical displacements (red) 367 s after rupture initiation (location indicated in Figure 1c). The Love wave ('L') dominates horizontal motion inducing displacements perpendicular to the propagation direction (SW). The Rayleigh wave ('R') dominates vertical motion inducing slight horizontal displacements parallel to propagation direction. We might see a superposition of surface waves due to multiple source asperities (dashed ellipse). (e, f) Permanent horizontal displacements of the earthquakes. (e) M_w9.0 (f) M_w7.9 and M_b6.7. Displacement of Figure 2e is subtracted from displacement field in Figure 2f.

rupture initiation. Since the propagation delay from the hypocenter to the nearest coastal sites is only about 15–20 s, we infer that the earthquake did not involve large slip for several tens of seconds after rupture initiation. This is confirmed by *Ide et al.* [2011], who show that the moment rate increased steeply from about 40–50 s after the rupture onset. At 67 s we see maximum horizontal and vertical offsets of 1.17 m and −0.31 m, respectively. Over the following 150 seconds the permanent displacement builds up to its maximum final displacement of 4.04 m of horizontal displacement and about 0.69 m of subsidence (see final displacements at 517 s in Figure 1a). Further details of the rupture process could be resolved from higher rate (e.g., 1 Hz) displacements. The induced dynamic displacements separate spatially from the permanent displacements from 217 s onwards, which shows that the significant permanent displacements are settled at the time the body waves have moved though and the rupture zone is defined (Figure 1 and Animation S3). At this time the NE and SW locations where the dynamic displacements intersect the coastline give an upper bound on the ruptured fault length. From this we can infer that the rupture process finished between 187 and 217 s and estimate a rupture zone length of about 530 km which compares well with *Simons et al.* [2011] who model a slip zone of about 500 km length. Given the rupture length and endpoints, a rapid inversion for rupture width and average slip, and thus seismic moment, is simple and could be done automatically.

[9] Following the main rupture at least two other events induce visible displacements (Figures 2e and 2f). At 06:09:30 UTC, 23:07 minutes after the M_w9.0 event, a small earthquake (likely M_b6.7, NEIC catalog, http://earthquake.usgs.gov/earthquakes/eqarchives/epic), induces significant horizontal displacement at several sites 200 km north of the main shock. This dynamic horizontal displacement reduces to considerably smaller, yet visible, permanent displacement in the next frame. The second event is M_w7.9 which ruptured at 06:15:40 UTC offshore of Tokyo. Identification of individual wave patterns is difficult, but S-waves and surface waves clearly propagate across the network.

4. Discussion and Conclusions

[10] We visualized for the first time the vector field of displacements induced by a large earthquake and associated

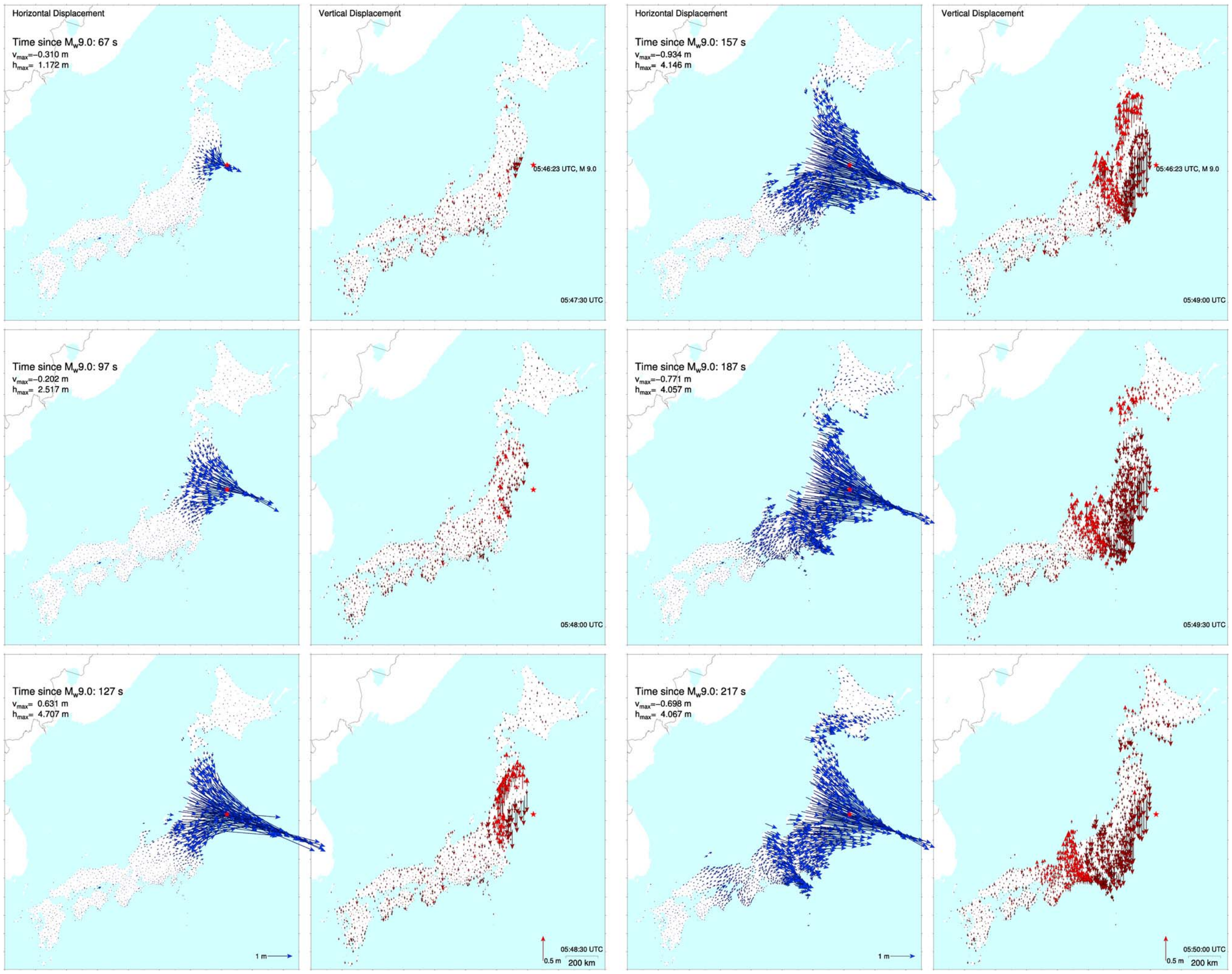

Figure 3. Evolution of permanent displacements due to the M_w9.0 rupture. Times are given relative to rupture initiation time. Blue and red arrows are horizontal and vertical displacements, respectively. Dark and light red indicate subsidence and uplift, respectively. Maximum vertical and horizontal displacements are given in the upper left corner of each row. First displacements appear at **67 s**. At **97 s** we see hardly any vertical deformation. The surface waves might mask permanent displacements of opposite direction. The vertical displacements at **127 s** support this as the waves radiate outward inducing uplift as their first motion. Furthermore, horizontal motion reaches its maximum displacement at 4.707 m. At **157 s** and **187 s** the horizontal dynamic wave pattern clearly separate from the permanent field. Vertical displacement reaches a maximum of −0.934 m at **157 s** indicating the negative phase of the Rayleigh wave passing through. At **217 s** the fully developed permanent displacement field is completely separated from the seismic waves (compare to Figure 1a).

aftershocks. We showed that map view visualizations of displacements recorded by dense, high-rate GPS networks can be used to directly estimate key characteristics of great earthquakes in near real-time. These time series of positions show the development of permanent and dynamic displacements related to long-period seismic waves. We acknowledge that some variations due to shorter-period seismic waves are likely aliased into the time-dependent displacement field and also note that seismic instrumentation is indispensable to fully understand the dynamics of events like the Tohoku-oki earthquake. We do, however, suggest automation of our approach and inclusion of the presented first order methods into subduction zone monitoring where dense GPS instrumentation exists. We hope the presented work will foster support of the work needed to expand dense GPS instrumentation along subduction zones following the example of Japan, Cascadia and California. Real time availability of these data is particularly important as induced ground displacements could be of great use in tsunami warning [*Blewitt et al.*, 2006, 2009], earthquake response, and perhaps earthquake early warning. In particular, the permanent displacements measured by GPS do not saturate at some maximum magnitude, as do the magnitude estimates typically used for rapid magnitude estimation in seismology. The feasibility to use real time GPS for such applications has been discussed and demonstrated in a number of studies. Using only real-time products for the analysis of the 2003 Tokachi-oki earthquake, *Yamagiwa et al.* [2006] demonstrate positioning precision on the order of a few centimeters. *Genrich and Bock* [2006] show that instantaneous, single-epoch positioning using ultra-rapid orbits yields horizontal precision of 6–10 mm and vertical precision of 40–50 mm for inter-station baselines of tens of kilometers, clearly demonstrating the fit of GPS for seismology applications. Such measured displacements displayed in map view in near real time give a direct first order estimate of the affected area. Convolution of dynamic and static displacements with functions that express, for example, ground composition or population density, will result in products similar to the Shake Maps created by the USGS which can be used in hazard response.

[11] The map view display of displacement data allows for instantaneous estimates of rupture duration (smaller than 217 s) and ruptured fault length (smaller than 530 km). The latter estimate is important to identify areas prone to large aftershocks as shown by the two strongest near coast aftershocks recorded within 30 minutes of the main event (Figures 2e and 2f). This length estimate, of course, scales with distance between landmass and thrust fault zone and will always be an overestimate when not corrected for this distance.

[12] After the body waves have moved through the near field at about 217 s, well before the tsunami hit the coast, we could have known that Japan's east coast subsided up to 60 cm, which puts the hinge line that separates subsidence from uplift offshore. This almost instantly suggests a complex mix of subsidence and uplift of the sea floor, which gives rapid insight into the tsunami potential as a large amount of energy went into water column displacement. The vertical displacements presented in map view also allow for a fast identification of the parts of the coastline now exposed to a raised mean sea level. Such changes in coastal topography have immediate implications for tsunami hazard mitigation as protective levees were effectively lowered by up to 60 cm. Furthermore, the M_{wp} earthquake magnitude scale used in some tsunami warning applications saturates at M_{wp} 8.0, but visualization of real-time GPS displacements would provide an immediate visual and quantitative indication of the difference between an earthquake of that size and an M_w9.0 event (Figures 2e and 2f). From this it would have been obvious that the initial estimate of M_w7.9 calculated about 3 minutes after onset of the rupture was a gross underestimate.

[13] Automation of our manual quantitative assessment is not hard to imagine. Combined with a self-organizing ad-hoc network approach as described by *Fleming et al.* [2009] a displacement based alarm system could be implemented. Alarm triggering would depend on evaluation of spatial and temporal consistency of the data. For temporal consistency a station needs to compare its current position to its displacement history, i.e., continuously increasing displacement in one direction between epochs suggests a physical process rather than noise. In parallel to this spatial consistency can be evaluated, which means a station could negotiate with its nearest neighbors whether they experience comparable position changes. Once consistency in displacements is assured an alarm can be triggered across the network providing redundancy to seismically triggered alarms.

[14] Lastly, showing three earthquakes of different magnitudes in one animation creates an accessible visualization of the meaning of earthquake size. Because displacements presented as vector fields in map view are more intuitive than velocities or accelerations shown in seismograms, visualizations like these can increase the understanding of earthquake mechanics and inform and educate policy makers, educators, and scholars alike.

[15] **Acknowledgments.** We thank C. Tape, D. Christensen, and A. Arendt for discussion of the earlier versions of the paper, and P. Haeussler and B. Atwater for comments on early versions of the animations. Two anonymous reviewers provided valuable feedback. All figures, including individual frames of the animations were created using the GMT public domain software [*Wessel and Smith*, 1995]. The authors express their gratitude towards the ARIA team at JPL and Caltech who provided preliminary GPS time series, and the GPS group at the Geospatial Information Authority (GSI) of Japan for operating GEONET and providing all original GEONET RINEX data to Caltech. We also thank the GEO Supersites team which enabled timely data and result exchange in the days and weeks after the earthquake. Financial support by the Alaska Volcano Observatory is acknowledged.

[16] The Editor thanks the two anonymous reviewers for their assistance in evaluating this paper.

References

Blewitt, G., C. Kreemer, W. C. Hammond, H.-P. Plag, S. Stein, and E. Okal (2006), Rapid determination of earthquake magnitude using GPS for tsunami warning systems, *Geophys. Res. Lett.*, *33*, L11309, doi:10.1029/2006GL026145.

Blewitt, G., C. Kreemer, W. C. Hammond, H.-P. Plag, S. Stein, and E. Okal (2009), GPS for real-time earthquake source determination and tsunami warning systems, *J. Geod.*, *83*, 335–343, doi:10.1007/s00190-008-0262-5.

Crowell, B. W., Y. Bock, and M. B. Squibb (2009), Demonstration of earthquake early warning using total displacement waveforms from real-time GPS networks, *Seismol. Res. Lett.*, *80*(5), 772–782, doi:10.1785/gssrl.80.5.772.

Fleming, K., M. Picozzi, C. Milkereit, F. Kühnlenz, B. Lichtblau, J. Fischer, C. Zulfikar, and O. Özel (2009), The Self-organizing Seismic Early Warning Information Network (SOSEWIN), *Seismol. Res. Lett.*, *80*(5), 755–771, doi:10.1785/gssrl.80.5.755.

Genrich, J. F., and Y. Bock (2006), Instantaneous geodetic positioning with 10–50 Hz GPS measurements: Noise characteristics and implications for monitoring networks, *J. Geophys. Res.*, *111*, B03403, doi:10.1029/2005JB003617.

Ide, S., A. Baltay, and G. C. Beroza (2011), Shallow dynamic overshoot and energetic deep rupture in the 2011 M_w 9.0 Tohoku-Oki earthquake, *Science*, *322*, 1426, doi:10.1126/science.120702.

Larson, K. M., P. Bodin, and J. Gomberg (2003), Using 1-Hz GPS data to measure deformations caused by the Denali fault earthquake, *Science*, *300*, 1421–1424, doi:10.1126/science.1084531.

Sagiya, T. (2004), A decade of GEONET: 1994–2003—The continuous GPS observation in Japan and its impact on earthquake studies, *Earth Planets Space*, *56*, xxix–xli.

Simons, M., et al. (2011), The 2011 magnitude 9.0 Tohoku-Oki earthquake: Mosaicking the megathrust from seconds to centuries, *Science*, *322*, 1426, doi:10.1126/science.120702.

Wessel, P., and W. H. F. Smith (1995), New version of the Generic Mapping Tools released, *Eos Trans. AGU*, *76*(33), 329.

Yamagiwa, A., Y. Hatanaka, T. Yutsudo, and B. Miyahara (2006), Real time capability of GEONET system and its application to crust monitoring, *Bull. Geogr. Surv.*, *53*, 27–33.

J. T. Freymueller and R. Grapenthin, Geophysical Institute, University of Alaska Fairbanks, PO Box 757320, 903 Koyukuk Dr., Fairbanks, AK 99775-7320, USA. (ronni@gi.alaska.edu)